Polar Cyclones at the Origin of the Reoccurrence of the Maud Rise Polynya in Austral Winter 2017

Diana Francis, Clare Eayrs, Juan Cuesta, David Holland

JGR Atmospheres

RESEARCH ARTICLE
10.1029/2019JD030618

Polar Cyclones at the Origin of the Reoccurrence of the Maud Rise Polynya in Austral Winter 2017

Diana Francis[1], **Clare Eayrs**[1], **Juan Cuesta**[2], **and David Holland**[1,3]

[1]New York University Abu Dhabi Research Institute, Centre for Global Sea Level Change, New York University Abu Dhabi, Abu Dhabi, United Arab Emirates, [2]Laboratoire Interuniversitaire des systèmes atmosphériques, CNRS and Université Paris-Est Créteil Val de Marne, Paris, France, [3]Center for Atmosphere Ocean Science, Courant Institute of Mathematical Sciences, New York University, New York, NY, USA

Abstract This study examines the role of atmospheric forcings in the occurrence of open-ocean polynyas by investigating the case of the austral winter 2017's polynya located in the Lazarev Sea sector to the east of the Weddell Sea, known as the Maud Rise polynya or the Weddell Polynya. The ice-free zone appeared in mid-September 2017 and grew to as large as 80,000 km^2 by the end of October 2017 before merging with the open ocean after the sea ice started to retreat at the beginning of the austral summer. Using a combination of satellite observations and reanalysis data at high spatiotemporal resolution, we found that severe cyclones, occurring over the ice pack, have a deterministic role in creating strong divergence in the sea ice field through strong cyclonic surface winds leading to the opening of the polynya. The occurrence of intense and frequent cyclones over the ice pack during austral winter 2017 was unusual, and it occurred under an enhanced strong positive meridional transport of heat flux and moisture toward Antarctica associated with an amplification of the atmospheric zonal wave 3 and a strong positive Southern Annular Mode index. We found that the opening of the polynya was not primarily due to direct ice melt by thermodynamic effects but rather to strong dynamical forcing by the winds on the sea ice, as in the case of coastal polynyas. Indeed, the meridional transport of heat toward Antarctica occurred over the Weddell Sea sector (i.e., to the east of the Lazarev Sea sector where the polynya is located) whereas the Lazarev Sea sector was under the influence of equatorward transport of cold air masses at that time. Our results show that the supply of warm and moist air coming from the west side of the South Atlantic Ocean into the Weddell Sea significantly increased the potential for cyclone formation as measured by the Eady growth rate leading to intense and frequent cyclogenesis over the ice pack, far south from the ice edge. After cyclogenesis in the Weddell Sea, these cyclones intensified as they moved eastward spinning over the Lazarev Sea with intensity comparable to category 11—violent storms—in the Beaufort scale. The cyclonic winds generated sea ice divergence by pushing the ice away from the cyclone center: To the east, north of it and to the west, south of it, which led to the reoccurrence of the Maud Rise polynya in mid-September 2017.

Key Points:
- Severe cyclones occurring over the ice pack have a deterministic role in the opening of midsea polynyas
- Strong cyclonic winds caused sea ice divergence, triggering the reoccurrence of the Maud Rise polynya in September 2017
- The formation of intense and frequent cyclones over the ice pack occurred under an amplified atmospheric zonal wave 3 pattern

Correspondence to:
D. Francis,
diana.francis@nyu.edu

Citation:
Francis, D., Eayrs, C., Cuesta, J., & Holland, D. (2019). Polar cyclones at the origin of the reoccurrence of the Maud Rise Polynya in austral winter 2017. *Journal of Geophysical Research: Atmospheres*, *124*. https://doi.org/10.1029/2019JD030618

Received 14 MAR 2019
Accepted 11 APR 2019
Accepted article online 24 APR 2019

Author Contributions:
Conceptualization: Diana Francis
Data curation: Clare Eayrs, Juan Cuesta
Formal analysis: Clare Eayrs
Funding acquisition: David Holland
Investigation: Diana Francis
Methodology: Diana Francis, Clare Eayrs
Software: Clare Eayrs
Supervision: Diana Francis
Visualization: Clare Eayrs, Juan Cuesta
Writing - original draft: Diana Francis
Writing – review & editing: Diana Francis

1. Introduction

Midsea winter polynyas that occur in the middle of the ice pack over certain oceanic-preconditioned areas around Antarctica have been intriguing features since they were first spotted in the satellite imagery in the 1970s. Several attempts to explain the underlying causes for the occurrence of open-ocean polynyas have been made in the past, but little attention has been given to the role of the atmospheric forcings in such phenomena. Here we shed light on the atmospheric triggers for the opening of the austral winter 2017's polynya located in the Lazarev Sea sector to the east of the Weddell Sea, known as the Maud Rise or the Weddell polynya (Figure 1). The ice-free zone appeared in mid-September 2017 with an areal extent of approximately 9,500 km^2 (Figure 1) and grew to as large as 80,000 km^2 by the end of October 2017 before merging with the open ocean after the sea ice started to retreat at the beginning of the austral summer.

Polynyas, defined as a stretch of open water surrounded by ice (e.g., Morales Maqueda et al., 2004), are frequently found near the Antarctic coast where strong katabatic winds push the ice offshore leading to open-water patches (i.e., Nihashi & Ohshima, 2015) and rarely in the midst of the winter sea ice pack. One such midsea polynya, found around Antarctica, occurs over the Maud Rise (Carsey, 1980; Mazloff et al., 2017; Reid et al., 2017). The Maud Rise in the Lazarev Sea provides an ideal location for the initialization of a midsea polynya. The rise is a seamount that climbs about 4,000 m to within 1,200 m of the surface

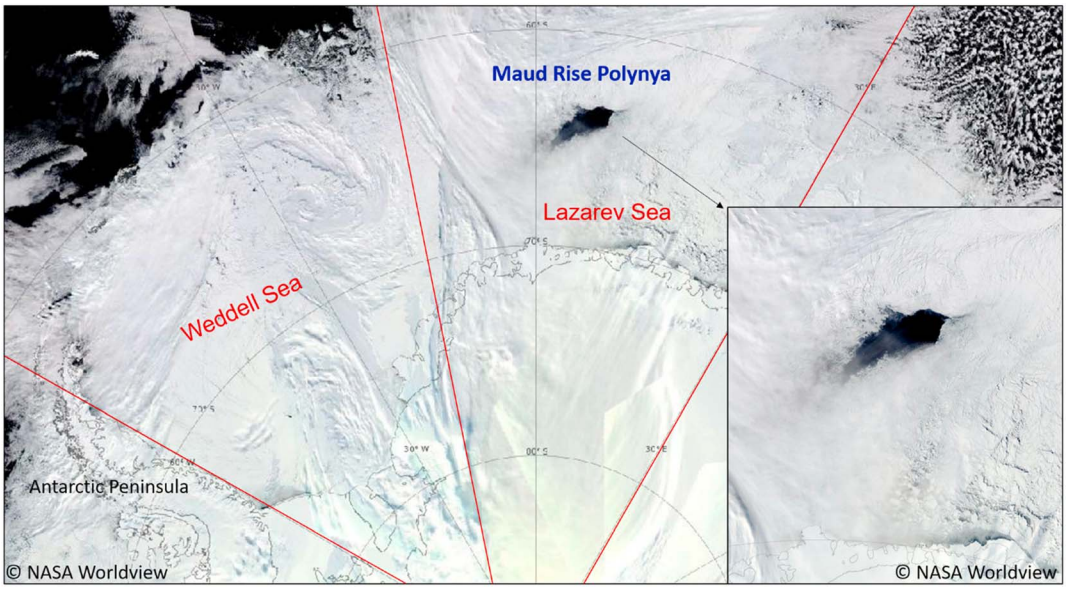

Figure 1. MODIS satellite visible imagery showing the location of the Maud Rise polynya in the Lazarev Sea to the east of the Weddell Sea and the Antarctic Peninsula. Satellite images are from NASA Worldview (https://worldview.earthdata.nasa.gov/) and adapted by the authors.

creating a semipermanent Taylor cap that brings middepth Weddell Deep Water to the surface (e.g., Dufour et al., 2017; Kurtakoti et al., 2018). In this area, the sea ice is thin in general and has low concentration even during winter months (e.g., Kurtakoti et al., 2018; Schlosser et al., 2018).

Once opened, the polynya works like a window through the sea ice, transferring huge amounts of energy between the ocean and the atmosphere. Unusual cloud formation is found over large midsea polynyas (i.e., Weijer et al., 2017), which makes them even more difficult to detect from space. Given their large size in the middle of the ice pack, midsea polynyas, through intense deep convection, are capable of impacting the climate locally, regionally, and potentially globally (e.g., Morales Maqueda et al., 2004) by modifying the oceanic circulation underneath (i.e., Gordon, 1998). This includes impact on the regional atmospheric circulation (e.g., Moore et al., 2002), the global overturning circulation (e.g., Martin et al., 2013, 2015), Antarctic deep and bottom water properties (e.g., Zanowski et al., 2015), and oceanic carbon uptake (Bernardello et al., 2014). Therefore, it is important to identify the triggers for the occurrence of midsea polynyas to improve their representation in the models, hence their predictability and associated feedbacks on the climate system.

Because Antarctica is a continent surrounded by ocean, sea ice can be spread freely by surface winds. These winds are strongly linked to weather systems (e.g., Schemm, 2018) which in turn are the result of the larger-scale climate variability (e.g., Pope et al., 2017). Recent studies have shown that surface winds are the key factor, both thermodynamically and dynamically, underlying the sea ice variability around Antarctica and can explain most of the observed interannual variability and sea ice trends (Holland & Kwok, 2012; Kwok et al., 2017; Matear et al., 2015; Schemm, 2018). For example, Schemm (2018) examined connections between sea ice extent and the frequencies of extratropical cyclones and blocks and showed that significant connections exist between weather systems and sea ice conditions in almost all regions that exhibit long-term sea ice trends during spring and autumn.

Swart et al. (2018) stated that in the lead-up to the 2017 polynya event, the Southern Annular Mode (SAM), which is the dominant mode of atmospheric variability in the extratropical Southern Hemisphere, was strongly positive with three of its 10 highest monthly values since 1957 recorded in 2015 and 2016, including the largest value in February 2015—coinciding with the annual sea ice minimum. They suggested that strong winds and an associated enhanced Weddell Gyre may have favored the right preconditions for a polynya event and concluded that more research is needed to better understand the respective roles of large-scale modes (SAM) versus regional circulation anomalies.

While several atmospheric phenomena can be at the origin of strong surface winds, inward spiraling winds generated by synoptic-scale cyclones are so powerful and cyclones of different types and

categories are considered to be the most powerful atmospheric features around the globe (e.g., Orlanski, 1975; Rudeva & Gulev, 2007) given their significant impacts on the environment on a synoptic scale as a result of the extremely high energy they carry (e.g., Bou Karam et al., 2010; Francis et al., 2018). This is particularly true in polar areas, where polar cyclones are intense and their impact on the surface is believed to be considerable (Kolstad, 2011; Rasmussen & Turner, 2003; Simmonds et al., 2008). In the Southern Hemisphere, where cyclonic winds spin clockwise, the highest wind speed occurs along the bent-back front of the cyclone, that is, to the left of the low-pressure center of the cyclone (Wagner et al., 2011; Watanabe & Niino, 2014).

Polar cyclones, both baroclinic and "convective" systems (i.e., "systems for which the main energy source is latent heat release in deep convection," Rasmussen & Turner, 2003, section 1.3), are known for their impact on the sea ice drift, fractioning, and redistribution. Several studies have demonstrated the important role of polar cyclones in the rapid creation of extreme sea ice conditions and that from a dynamical point of view, more frequent and intense cyclones result in more fragile and less consolidated ice edge. (e.g., Bromwich et al., 2011; Kwok et al., 2017; Turner et al., 2002; Wang et al., 2014). These findings attest to the strong impact that cyclone-induced winds can have on the sea ice drift and redistribution. The preferred region for cyclogenesis is generally where both a strong temperature gradient and an upper-level trough are found (e.g., Davies, 1997; Shimada et al., 2014; Uccellini, 1990). Around Antarctica, the strongest temperature gradient is found along the fringes of the ice pack, making the sea ice edge a preferred region for cyclogenesis (e.g., Schlosser et al., 2011; Stoll et al., 2018; Yanase & Niino, 2007). High baroclinic instability associated with the horizontal temperature gradient is crucial for the formation and the intensification of the cyclones (Davies, 1997; Uccellini, 1990; Yanase & Niino, 2007), but cyclogenesis occurs only at the entrance and exit regions of upper-level troughs (e.g., Kolstad, 2011; Shimada et al., 2014).

However, the location of the temperature gradient relative to the ice edge depends strongly on the general atmospheric conditions at large scale. Of particular importance is the meridional heat and moisture transport that can be characterized by looking at the zonal wave number 3 (ZW3) pattern in the general circulation around Antarctica (Raphael, 2004). The amplitude of ZW3 is an indication of the larger-scale temperature gradient so that high amplitudes of ZW3 are associated with steeper temperature gradients. The ZW3 (together with zonal wave 1, ZW1) describes the asymmetry in the generally strongly zonally symmetric circulation of the extratropical Southern Hemisphere. Both ZW1 and ZW3 have preferred regions of meridional flow, guiding the meridional transport of heat and moisture into and out of the Antarctic. ZW1 and ZW3 vary with each other so that when ZW3 is strong, ZW1 is weak, and vice versa. Although the amplitude of the wave is highest near 49°S (e.g., Hurrell et al., 1998; van Loon & Jenne, 1972) the southern edges of the wave extend far enough south to influence the sea ice field. Where the anomaly is positive (in the ridges) the flow is expected to be counterclockwise and diverging, and where it is negative (in the troughs) the flow is expected to be clockwise and converging (Raphael, 2007). This results in regions of preferred northerly (poleward) and southerly (equatorward) flow whose locations are strongly influenced by the phase of ZW3. ZW3 forces an alternating pattern of equatorward (colder) and poleward (warmer) flow which influences the temperature difference between the different sectors. An index of ZW3 based on its amplitude defined by Raphael (2004) shows that ZW3 has positive and negative phases, where a positive phase indicates strong meridional flow and a negative phase more zonal flow. van Loon and Jenne (1972) and Raphael (2007) show that the annual cycle of the ZW3 has a maximum in austral winter and a minimum in spring.

Through the meridional transport of heat and moisture, the ZW3 influences the variability of Antarctic sea ice both dynamically and thermodynamically. Schlosser et al., 2018 showed that the early onset of melt and the rapid decrease in sea ice area and sea ice extent in 2016 were associated with atmospheric flow patterns related to a positive ZW3 index, that is, synoptic situations leading to strong meridional flow and anomalously strong southward heat advection in the regions of strongest sea ice decline. Increased warm air advection toward Antarctica triggered the negative Antarctic sea ice anomaly in 2016 and 2017. Irving and Simmonds (2015) found that ZW3-like anomalous states are associated with large precipitation anomalies linked to convective systems over coastal Antarctica. Raphael (2007) and Raphael and Hobbs (2014) showed that the influence of ZW3 on sea ice concentration (SIC) appears greatest in the southern fall and early winter. Among the regions that are strongly influenced by the ZW3 is the Weddell Sea where positive correlations with the ZW3 index were found, whereas the strongest negative correlations occur in the

Lazarev Sea. They explained this negative correlation by the fact that their analysis did not take into account the role of strong wind and storms on the SIC. Moreover, Raphael (2007) concluded that the influence of the surface winds associated with ZW3 on SIC and redistribution has not been analyzed and suggested that anomalous wind direction associated with a strong ZW3 could have a great influence on the sea ice advection. This is in agreement with the recent findings by Schemm (2018) who stressed the role of anomalous winds associated with low and high pressure systems on the sea ice extent and the spatial and temporal connections.

Building on these studies that investigated separately the link between atmospheric ZW3 pattern and sea ice conditions and the role of cyclones in sea ice dynamics, we aim in this study to establish the link between cyclone activity and sea ice dynamics leading to the occurrence of the polynya and to highlight the role of the ZW3 pattern in both cyclone activity and polynya occurrence.

The role of atmospheric forcings in the opening of the Maud Rise polynya 2017 under a ZW3-like situation is investigated in this study using satellite data for the sea ice characterization and atmospheric reanalyses to describe the synoptic conditions during the austral winter months July to September 2017. The data used are described in section 2. The general atmospheric conditions at synoptic scale are addressed in section 3. In section 4, we investigate the atmospheric dynamics during the period 13–16 September when the polynya first opened, and we characterize the composition of the atmosphere above the polynya in section 5. Section 6 summarizes our findings.

2. Data

2.1. Reanalyses Data

European Centre for Medium-Range Weather Forecasts Interim reanalysis (ERA-Interim) data were used to investigate the synoptic atmospheric conditions during the austral winter 2017 relative to the climatological record. These reanalysis data are available from 1 January 1979 to present at 6-hourly intervals (0000, 0600, 1200, and 1800 UTC). The spatial resolution is T255, corresponding to approximately 79 km, with 60 vertical levels to 0.1 hPa. A detailed description of ERA-Interim is given in Dee et al. (2011).

The ERA-Interim data were used to plot normalized anomalies of mean sea level pressure (MSLP), temperature, and vertically integrated equatorward heat flux, derived from the monthly mean values. To calculate the normalized anomalies, we subtracted, for a given variable, the monthly climatological mean from the monthly means in 2017, and we divided that by the standard deviation of the climatology. The monthly climatology in our case was created from the 1979–2017 ERA-Interim monthly data set. We also used the daily ERA-Interim MSLP and geopotential heights at 500 hPa data to calculate the ZW3 Index based on Raphael (2004) at the three ridges: latitude 45°S and longitudes 79.5°E, 32.25°W, and 139.5°W, for 2017, 2016 (daily for the whole year) and for July-August-September (JAS) months across the full record 1980–2017. The index has both positive and negative phases, where a positive index indicates more meridional flow (larger amplitude ZW3) and a negative index indicates more zonally oriented flow (smaller amplitude ZW3; Raphael, 2004, 2007).

To investigate in detail the atmospheric dynamics that triggered the opening of the polynya, we used the ERA 5 reanalysis (Hersbach & Dee, 2016) for their higher temporal and spatial resolution (hourly at approximately 31 km with 137 levels to 0.01 hPa). ERA5 also has a more recent model and data assimilation system. At the time of this study, these data are only available from 1 January 2008 to present, so these cannot yet be used for climatological studies.

Furthermore, a measure for the potential development and intensification of low-pressure systems has been proposed by Eady (1949). The Eady model describes the growth of midlatitude eddies, and the maximum Eddy Growth Rate comprises a combination of vertical stability and vertical wind shear and describes how well deep pressure systems can develop in a synoptic situation over a specific area (e.g., Lindzen & Farrell, 1980). The Eady growth rate is given by

$$\sigma_E = 0.3098|f|\frac{\left|\frac{\delta U(z)}{\delta z}\right|}{N}$$

where f is the Coriolis parameter, N is the Brunt Väisällä frequency, U is the horizontal wind speed, and z is the vertical height. The Eady growth rate, with units of per day, is a measure of the

instability of the atmosphere to baroclinic disturbances. In our analysis we used the atmospheric layer between 850 and 500 hPa.

2.2. Satellite Data

SICs were obtained from the National Oceanic and Atmospheric Administration/National Snow and Ice Data Center Climate Data Record (CDR) of Passive Microwave Sea Ice Concentration, Version 3 (Meier, Fetterer, Savoie, et al., 2017; Meier, Fetterer, & Windnagel, 2017) and its near-real-time version (Meier, Fetterer, Savoie, et al., 2017; Meier, Fetterer, & Windnagel, 2017). The near-real-time CDR is designed to fill the temporal gap between updates of the final CDR. These data are on the National Snow and Ice Data Center polar stereographic grid with nominal 25 × 25-km grid cells at both daily and monthly temporal resolutions. These products comprise data from the NASA Team algorithm (Cavalieri & Parkinson, 2008) and the Bootstrap algorithm (Comiso, 1986), as well as a merged data set. The bootstrap algorithm performs better than the NASA Team algorithm around Antarctica, but the Bootstrap algorithm potentially underestimates the concentration of sea ice in the presence of thin ice (Comiso et al., 1997), so we used the merged product, which should be more accurate in our region of interest. The 15% contour in the SIC was used to determine the sea ice extent and to delineate the polynya. For the information on the vertical structure and composition of the atmosphere above the polynya area, we used the Cloud-Aerosol Lidar and Infrared Pathfinder Satellite Observation (CALIPSO; Cuesta et al., 2009; Winker et al., 2003).

To check the motion in the sea ice field around the polynya area, we used the low-resolution sea ice drift product of the EUMETSAT Ocean and Sea Ice Satellite Application Facility (www.osi-saf.org). This is a 2-day (48-hr) gridded ice drift data set processed on a daily basis and made available on a 62.5-km Polar Stereographic Grid (e.g., Kwok et al., 2013, 2017). Ice motion vectors are estimated by an advanced cross-correlation method on pairs of satellite images (Lavergne et al., 2010). We used the multi-sensor spatial covering product that combines the Special Sensor Microwave Imager/Sounder (SSMIS, 91GHz H&V pol.) on board the Defense Meteorological Satellite Program (DMSP) platform F17, the Advanced SCATterometer (ASCAT, C-band backscatter) on board The European Organisation for the Exploitation of Meteorological Satellites (EUMETSAT) platform Metop-A, and the Advanced Microwave Scanning Radiometer 2 (AMSR2) on board the Japan Aerospace Exploration Agency (JAXA) platform GCOM-W. Due to atmospheric noise and surface melting, these data are only available for the Southern Hemisphere winter (1 April to 31 October).

3. General Atmospheric Conditions During Austral Winter 2017

The MSLP field in the high southern latitudes is dominated by the circumpolar trough across 60–70° S. Within this band there are three climatological low pressure centers located close to 20°E, 90°E, and 150°W (e.g., Turner et al., 2002). The location and depth of the three surface lows has a strong influence on the climatic conditions in the Antarctica coastal region.

During austral winter (JAS) 2017, the synoptic conditions exhibited an amplified ZW3 pattern. The broad scale MSLP anomaly pattern shown in Figure 2a indicates that for JAS 2017 there was below average pressure around much of the Antarctic continent and above average pressure to the north. The amplified wave number 3 pattern can be identified by its three trough/ridge systems associated with high MSLP anomalies located over the three sectors: South Atlantic, South Pacific, and Southeast Australia (Figure 2a). The most pronounced trough/ridge system was between 90°W and 0°E where MSLP anomalies exceeded one standard deviation from the mean over large areas with the strongest ridge seen over the Southwest Atlantic Ocean and troughing over the Antarctic Peninsula and the surrounding seas (Figure 2a).

Normalized anomalies of 2-m temperature over the JAS 2017 period are shown in Figure 2b. Anomalous warm air masses appear to be associated with the high pressure anomalies areas discussed earlier and the same wave 3 pattern can be seen in the temperature field as well (Figure 2b). Temperature anomalies exceeded two standard deviations from the mean, particularly in the South Atlantic and the South Pacific sectors. The amplified ZW3 circulation resulted in strong zonal temperature gradients at the boundary between meridional warm and cold air masses (to the west of the Antarctic Peninsula and at 0°E, e.g., Figure 2b). Such frontal areas between two different air masses with strong temperature gradients are known to favor baroclinic instability, wind shear, and therefore cyclogenesis (e.g., Yanase & Niino, 2007).

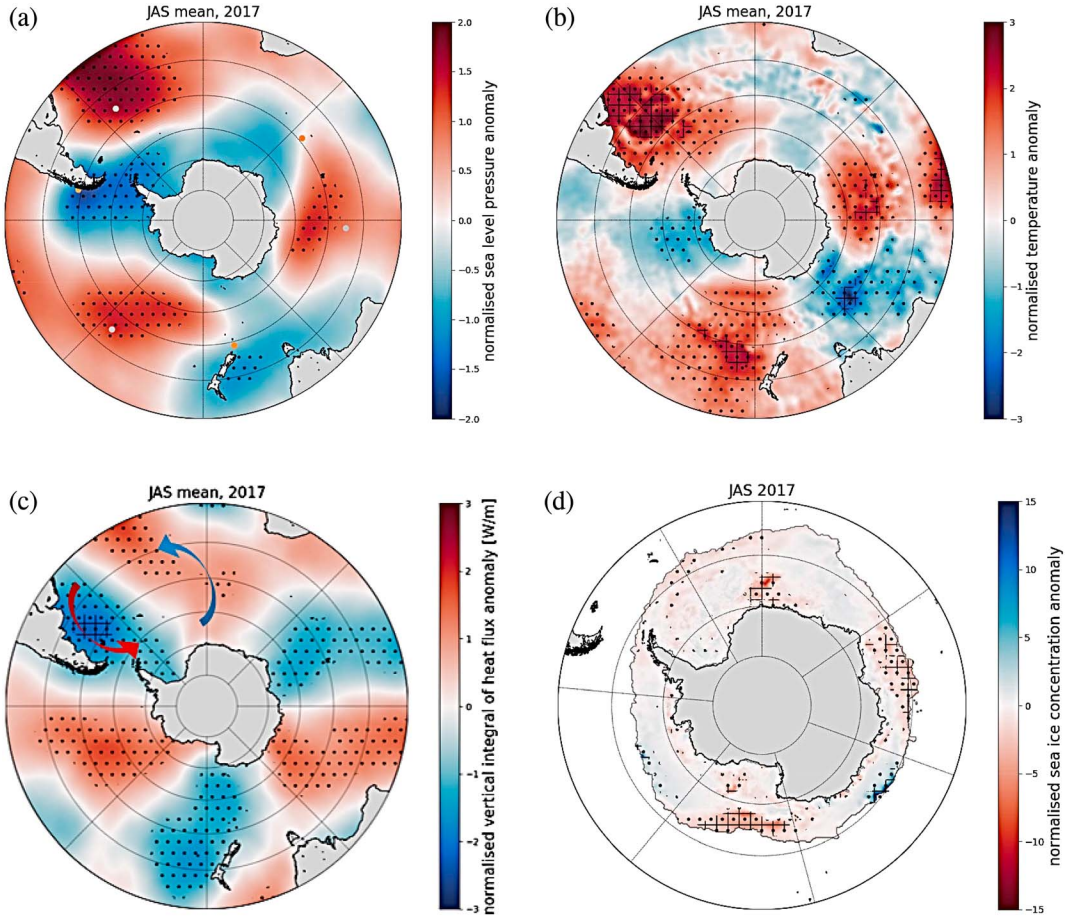

Figure 2. Normalized anomalies for the period July-August-September (JAS) 2017 of European Centre for Medium-Range Weather Forecasts Interim Reanalyses of mean sea level pressure (a), 2-m temperature (b), vertical integral of meridional heat flux (c), and sea ice concentration anomalies for JAS 2017 from AMSR2 (d). Black dots are regions where the normalized anomalies are larger than one standard deviation from the mean, and black squares are regions where the normalized anomalies are larger than two standard deviations from the mean. The orange dots in (a) are the three locations that Raphael (2004) used for the ZW3 index calculation; the gray dots in (a) are the three locations that we used to calculate the ZW3 corresponding to the position of the three pressure ridges during JAS 2017. The red arrow in (c) represents the poleward transport of warm air, and the blue one represents the equatorward transport of cold air.

The amplification of the ZW3 is associated with more meridionality in the otherwise zonal flow manifested through the deeper troughs and higher ridges of the ZW3, with northerly and southerly flows along each side (e.g., Schlosser et al., 2018). Such conditions result in poleward transport of warm air and equatorward transport of cold air. In Figure 2c, the normalized anomalies of the vertically integrated equatorward heat flux from ERA-Interim are displayed. Positive values suggest equatorward transport of cold air, and negative values show poleward transport of warm air toward Antarctica. The pattern in the heat flux is consistent with the spatial temperature distribution around Antarctica discussed in Figure 2b. A strong signal in the vertically integrated meridional heat flux is seen off the west coast of South America where anomalies exceeded two standard deviations from the mean suggesting a significant warm air transport toward the Antarctic Peninsula over the JAS period (Figure 2c). The transport of air masses from and toward Antarctica are consistent with the disposition of high and lows seen in the MSLP anomalies field (Figure 2a).

Figure 2d shows the normalized anomalies of SIC for the same period. Less than average SICs are seen in areas where enhanced poleward transport of warm air is occurring except over the Lazarev Sea where strongly negative anomalies occurred under conditions of equatorward transport of cold air (Figures 2b–2d) inferring a dynamical impact of the circulation on the sea ice field in this area rather than thermodynamically driven one (i.e., direct ice melt as in the other sectors). This result is in phase with earlier findings by Raphael and Hobbs (2014). We note also that in the Weddell Sea sector, where strong transport of warm air is occurring

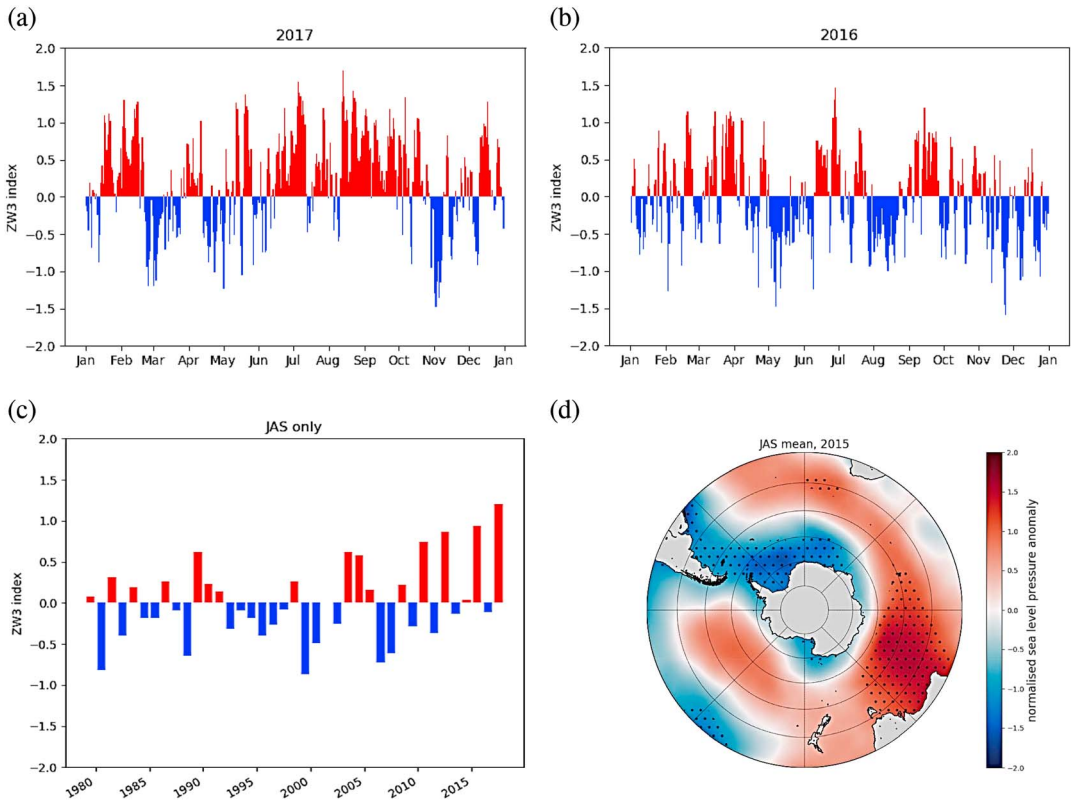

Figure 3. ZW3 index calculated from daily geopotential height at 500 hPa based on Raphael (2004) at the three ridges (latitude 45°S and longitudes 79.5°E, 32.25°W, and 139.5°W, gray dots in Figure 2a) for 2017 (a), 2016 (b), and for July-August-September months only for the full record 1980–2017 (c). Normalized anomalies for the period July-August-September (JAS) 2015 of European Centre for Medium-Range Weather Forecasts Interim Reanalyses of mean sea level pressure (d).

(i.e., Figures 2b and 2c), the SIC anomalies do not exhibit remarkable changes in contrast to the Ross Sea and Indian Ocean sectors where negative anomalies exceeded two standard deviations from the mean in the areas under the influence of warm air masses. The excess in warmth and energy in the Weddell Sea sector seems to be the result of the formation of frequent and strong cyclones that propagate poleward and then eastward favored by orographic blocking, as will be discussed in the following section.

The MSLP, temperature, and meridional heat advection shown in Figure 2 all have a clear signal of ZW3 pattern. Given these patterns, we examine the ZW3 index calculated from daily geopotential height at 500 hPa based on Raphael (2004) at the three ridges (latitude 45°S and longitudes 79.5°E, 32.25°W, and 139.5°W) for which the position is shown by gray dots in Figure 2a. The ZW3 index was calculated for the whole year in 2017 and 2016 and only for JAS months for the full record 1980–2017. The results are shown in Figure 3. The year 2016 is shown to put 2017 into perspective. In 2017, the ZW3 index was almost continuously positive over a longer time period compared to 2016 which in turn exhibited positive ZW3 index compared to previous years (e.g., Schlosser et al., 2018). Continuous positive ZW3 index was predominant in 2017 from June to October. Figure 3c shows the ZW3 index for the JAS period over the full record. The ZW3 index for JAS 2017 is the most positive of all years. The persistent positive ZW3 index during winter months in recent years (i.e., 2015 and 2014) and even more pronounced one in 2017, indicates that the sea ice may have preconditioned for polynya occurrence by favorable meridional heat flux transport conditions for ice melt and thinning during previous years (e.g., Clem et al., 2017; Raphael, 2007; Schlosser et al., 2018).

The synoptic situation in winter 2017 was unique and has not occurred in previous winters, for instance, in 2015, when the ZW3 index was only slightly lower than in 2017 (Figure 3c). MSLP anomalies for winter 2015 (Figure 3d) and winter 2016 (not shown) do not exhibit strong ZW3 pattern as discussed for winter 2017 earlier. This indicates that the meridional transport of heat was exceptional in winter 2017 when the polynya occurred.

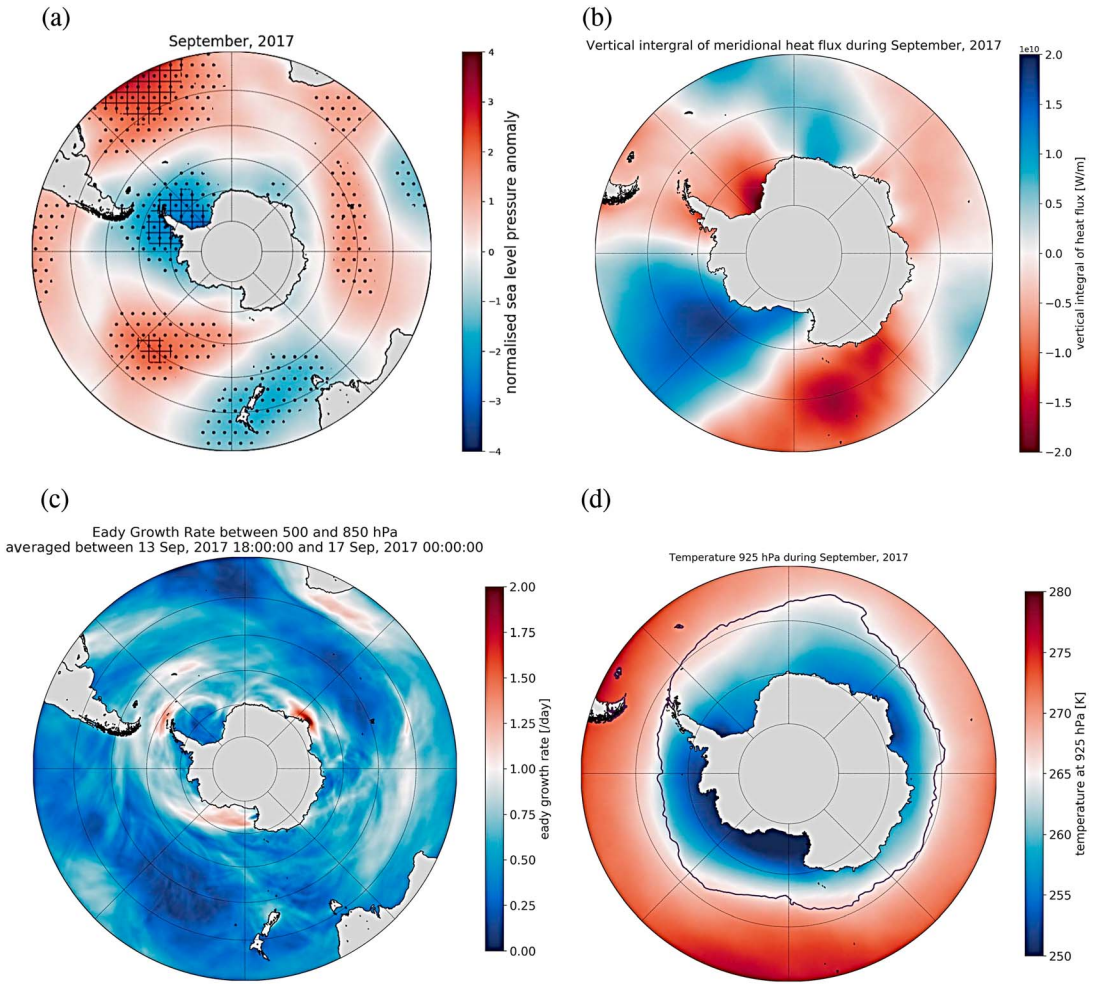

Figure 4. European Centre for Medium-Range Weather Forecasts Interim Reanalyses for the month of September 2017 of (a) normalized anomaly of mean sea level pressure, (b) monthly mean of vertically integrated meridional heat fluxes (positive equatorward, negative poleward) for the month of September 2017, and (c) Eady growth rate between 500 and 850 hPa calculated from hourly values averaged over the period 13 and 17 September 2017. (d) Monthly mean of temperature at 925 hPa. Black dots in the anomaly fields are regions where the normalized anomalies are larger than one standard deviation from the mean, and black squares are regions where the normalized anomalies are larger than two standard deviations from the mean. The purple line in (d) represents the monthly mean sea ice extent for September 2017 from AMSR2 3.125-km sea ice concentrations.

After addressing the general atmospheric conditions during the winter season, we now focus on the month of September 2017 during which the polynya first occurred. Figure 4a shows the normalized anomalies of MSLP for the month of September 2017. The ZW3 pattern stands out clearly in the anomalies field with the most pronounced trough/ridge over the Antarctic Peninsula and its surrounding seas and the South Atlantic, respectively. In this sector, both negative and positive normalized anomalies exceeded two standard deviations from the mean implying extremely anomalous conditions relative to the climatology. The strong ridge associated with the ZW3 pattern is located further south than usual and can favor a blocking situation over the Lazarev Sea associated with the high pressure area to the north of it (Figure 4a). The vertical integral of meridional heat flux shown in Figure 4b for the month of September 2017 indicates a significant transport of heat from South America and the eastern side of the South Atlantic Ocean toward the Antarctic Peninsula and the Weddell Sea, whereas equatorward transport of cold air masses was observed to occur over the Lazarev Sea (Figure 4b). Examining the Eady growth rate between 500 and 850 hPa (Figure 4c), a patch of high rates (1 to 1.25 per day) appears over the southwest Atlantic stretching toward the Weddell Sea, to the west of 0°. These results suggest an environment favorable for cyclogenesis and potential for development of cyclones over this area which is located over the ice-pack, south of the ice edge (Figure 4d).

In 2017, the SAM index was strongly positive as well as for the JAS 2017 (0.42 for September 2017, not shown), in favor of the strengthening of circumpolar westerlies and more cyclogenesis over Antarctic Peninsula (e.g., Lubin et al., 2008; Swart et al., 2018). This was calculated using the method by Marshall (2003), where a large (small) meridional pressure gradient means a positive (negative) SAM index and, correspondingly strong (weak) westerlies. It is known that the frequency of polar cyclones in the Antarctic Peninsula region (including the Weddell Sea) is correlated with the (SAM) index, most strongly during winter and spring (Lubin et al., 2008) and that during periods of positive SAM index, more cyclogenesis over the West Antarctica Peninsula is found.

Because of the pronounced ZW3-like situation in the Weddell Sea, the meridional temperature gradient, which is usually located near the ice edge, is seen to occur south of the ice edge over the ice pack in the Weddell Sea during the month of September 2017 (Figure 4d). This means that the atmospheric dynamics and forcings, such as deep cyclones, which normally occur near the ice edge, can now occur over the ice pack and impact the sea ice field. A strong zonal temperature gradient is seen at the boundary between warm and cold air masses near 0° (Figures 4b and 4d), and it persists throughout the month. This frontal zone associated with high baroclinic instability favors the occurrence and the maintenance of intense cyclones (e.g., Reed, 1979; Reed & Duncan, 1987; Schemm & Sprenger, 2015) that could exert dynamical forcing on the ice pack and open the polynya as will be shown in the following section.

In summary, the atmospheric conditions in 2017, associated with a strongly positive SAM index and an amplified atmospheric ZW3 characterized by strong meridional transport of heat, are thought to impact the sea ice conditions in several ways: (1) the enhancement of strong zonal temperature gradients between the different sectors leading to baroclinic instability that generates dynamically strong storms which in turn impacts the sea ice dynamics; (2) the formation of intense and frequent storms that are able to reach further south and penetrate deeper over the ice pack; and (3) the shift of the horizontal temperature gradient (and the cyclones that form across it) south of the ice edge in the Weddell Sea, which makes it possible for cyclones to form over the ice pack and force the sea ice conditions.

4. Atmospheric Dynamics Leading to the Opening of the Polynya

After having investigated the large-scale general atmospheric conditions during JAS 2017 with focus on September 2017 in the previous section, we now consider the local atmospheric dynamics that preceded and accompanied the opening of the polynya on 13–16 September.

The Weddell Sea can be seen as an active cyclogenesis zone during this period as a result of the intrusion of warm and moist air masses in combination with orographic blocking along the Antarctic Peninsula. Several cyclones can be seen forming at the same time (Figure 5a), deepening as they propagate eastward and spinning over the Lazarev Sea with surface-cyclonic winds exceeding 25 m/s (Figures 5b and 5c). For comparison, katabatic winds at the origin of the coastal polynyas, are associated with wind speeds of 10 m/s on average (e.g., Nihashi & Ohshima, 2015). On 13 September, an intense cyclone comparable to a category 11 storm (violent storm) in the Beaufort scale, associated with a center of low pressure deeper than 950 hPa (Figure 5a) entered the Lazarev Sea from the west and was blocked over 65–70°S/0–5°E for more than 12 hr by the ridge located to the northeast of the low that was emanating from the South Atlantic intense high (pressure exceeded 1,030 hPa) centered at 30°S/15°W (Figure 5a). The cyclone was associated with extremely strong surface winds exceeding 24 m/s and reaching in some areas 30 m/s (Figure 5b). The SICs before the arrival of the cyclone on 13 September were between 60% and 80% over the Maud Rise (Figure 5b), an area known for its thin and less concentrated ice due to the bathymetry of the seafloor and associated water dynamics (e.g., Dufour et al., 2017; Holland, 2001; Kurtakoti et al., 2018). The cyclone remained stationary over the Maud Rise area and its associated center at 66°S for almost 12 hr and strong cyclonic winds were able to exert dynamical forcing on the ice for a significant period of time leading to an open-water area on 14 September (Figure 5c). Sea ice drift data from 12 to 14 September 2017 derived from satellite observations are shown in Figure 5d. The sea ice north of 66°S is seen to drift to the east at speeds exceeding 60 km over 48 hr on average (Figure 5d), whereas the sea ice south of 66°S is seen to drift to the west with average speeds of 40 km per 48 hr (Figure 5d). As a consequence of the divergence in the horizontal motion of the ice induced by the cyclonic winds, an ice-free area appeared in the SIC field (Figure 5c). The polynya opened over the Maud Rise immediately after the center of the cyclone had

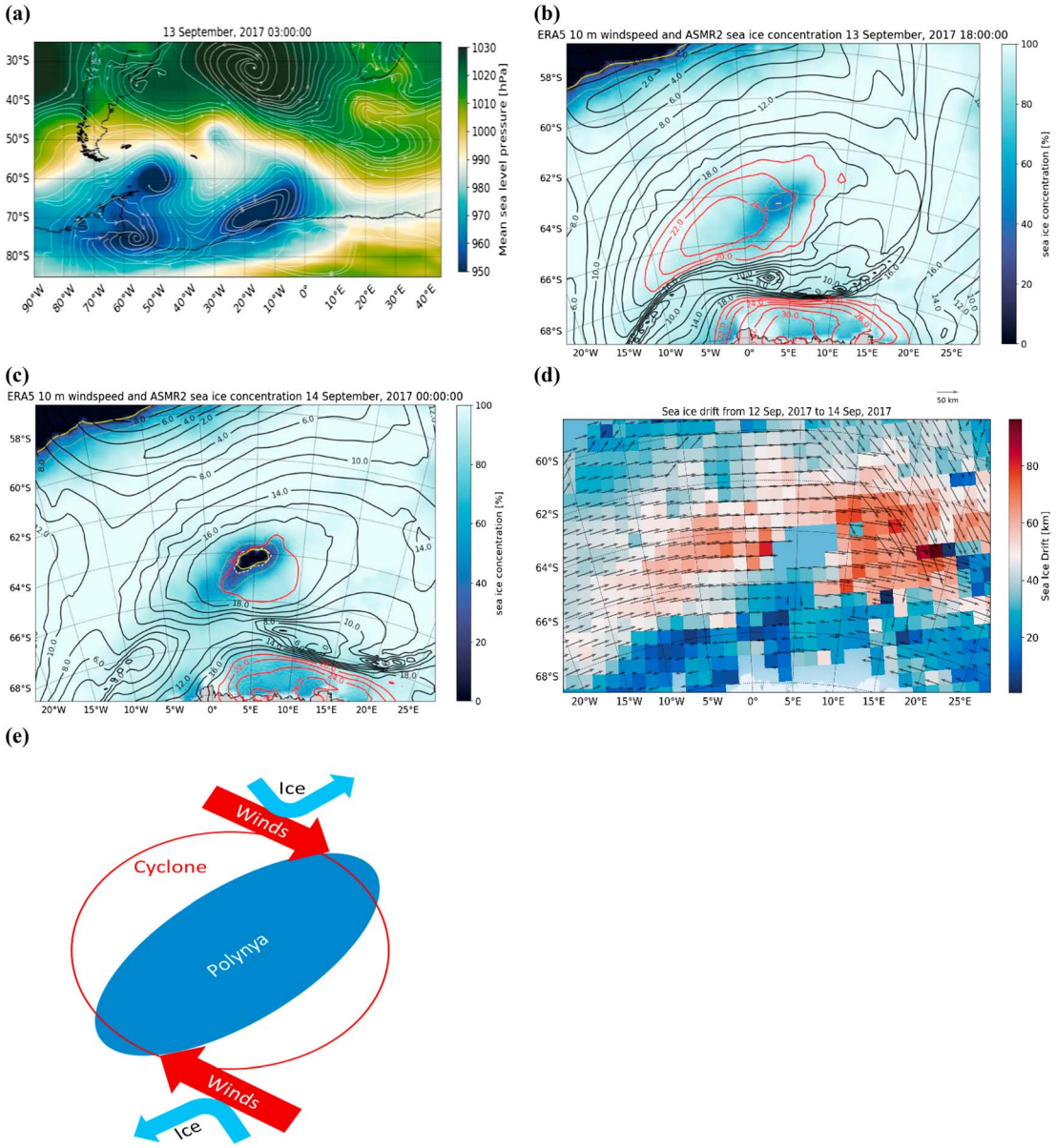

Figure 5. ERA 5 reanalyses of mean sea level pressure and wind direction at 925 hPa in streamlines on 13 September 2017 at 0300 UTC (a). AMSR2-derived sea ice concentrations on 13 September 2017 at 1800 UTC (b) and on 14 September 2017 at 0000 UTC (c). (d) Satellite-derived sea ice drift speed (shaded colors) and direction (vectors). (e) Sketch summarizing the mechanisms by which the cyclone opens the polynya. In (b) and (c) the black contours are ERA5 10-m winds less than 20 m/s, the red contours are ERA5 10-m winds 20 m/s and greater, the solid yellow contour is the 15% ERA-Interim sea ice contour, the dotted yellow contour is the 50% ERA-Interim sea ice contour, and the dashed white contour is the 15% ice from satellite data. ERA = European Centre for Medium-Range Weather Forecasts Re-Analysis.

moved further east (Figure 5c). The cyclone-induced strong winds of about 20 m/s were still observed over the polynya on 14 September (Figure 5d) to the left of the cyclone center, leading to a larger polynya the following days (not shown). Strong winds associated with the cyclone continued to redistribute the ice in a divergent motion around the polynya over the following days (not shown), which led to an even larger region of open water (i.e., Figure 6d).

The cyclonic nature of the winds is crucial to trigger the opening of a midsea polynya by creating divergence in the sea ice field. A conceptual sketch summarizing the action that cyclonic winds exert on the sea ice drift is displayed in Figure 5e. Leppäranta (2011) summarized the scientific knowledge on the drift of sea ice under the influence of both the atmospheric and the oceanic layers. He confirmed findings by previous

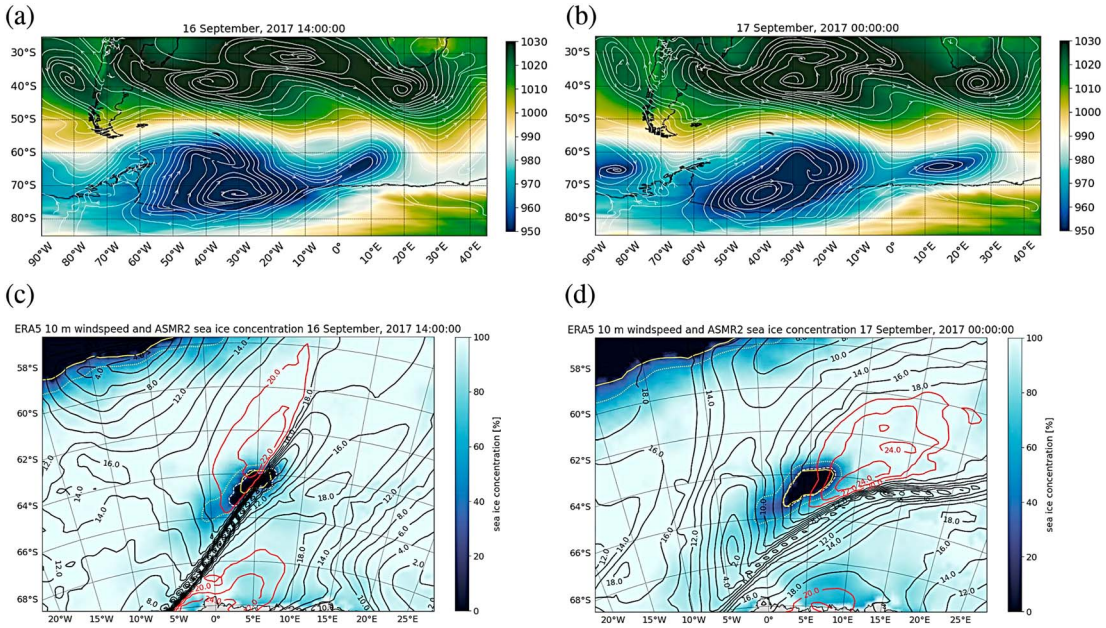

Figure 6. ERA 5 reanalyses of MSLP and wind direction at 925 hPa in streamlines on 16 September 2017 at 1400 UTC (a) and on 17 September 2017 at 0000 UTC (b). AMSR2-derived sea ice concentrations on 16 September 2017 at 1400 UTC (c) and on 17 September 2017 at 0000 UTC (d). In (c) and (d) the black contours are ERA5 10-m winds less than 20 m/s, the red contours are ERA5 10-m winds 20 m/s and greater, the solid yellow contour is the 15% ERA-Interim sea ice contour, the dotted yellow contour is the 50% ERA-Interim sea ice contour, and the dashed white contour is the 15% ice from satellite data delineating the polynya area. The yellow line in (c) shows the Cloud-Aerosol Lidar and Infrared Pathfinder Satellite Observation track on 16 September 2017 at 1400 UTC. ERA = European Centre for Medium-Range Weather Forecasts Re-Analysis.

studies where the direction of the ice drift is turned 30° on average to the left of the atmospheric flow (Kottmeier et al., 1992; Kottmeier & Sellmann, 1996; Leppäranta, 2011; Nansen, 1902) and the velocity of the ice drift amounts to 1–2% of the surface wind speed (e.g., Kottmeier et al., 1992; Leppäranta, 2011). Those results, when applied to a cyclonic winds situation (i.e., two opposing winds around a center), imply divergence in the motion of sea ice leading to open water area theoretically colocated within the cyclone center (Figure 5e).

The same prevailing conditions described earlier continued to affect the Weddell and Lazarev Seas during the following few days. A large and deep low (pressure less than 950 hPa at its center at 70°S/35°W) is seen to extend along the coast of the Weddell Sea on 16 September 2017 covering an area encompassing more than 40° in longitude and 15° in latitude (Figure 6a). A trough emanating from this low was seen to develop over the Lazarev Sea stretching as far east as 15°E. This deep trough developed later into a strong cyclone over the polynya area (Figure 6b). On both sides of the trough, strong surface winds exceeding 20 m/s can be seen resulting in strong convergence associated with nearly 0 m/s winds along the trough (Figure 6c). When the trough reached the Maud rise area, the polynya had already been opened by the cyclone on 13 September, but after the passage of the trough and associated winds the polynya was seen to increase in size (Figure 6d) under the effect of dynamical forcing by the strong surface winds. It is interesting to note that the shape of the polynya (Figure 6d) is aligned with the shape of the pressure low (Figure 6b), inferring the direct role of the strong opposing winds on both sides of the low in triggering the opening of the polynya, as also illustrated in Figure 5e.

Strong winds associated with the cyclone that developed from the deep trough on 17 September continued to redistribute the ice field. Strong divergence pushing the ice away from the polynya area led to an increased region of open water in the following days (not shown), which was then maintained open throughout the winter months by ocean dynamics.

Based on this analysis we conclude that the divergence in the sea ice field induced by cyclonic winds occurring over the Maud Rise—a preconditioned area in terms of SIC and ocean dynamics—led to the opening and the enlargement of the Maud Rise polynya in mid-September 2017.

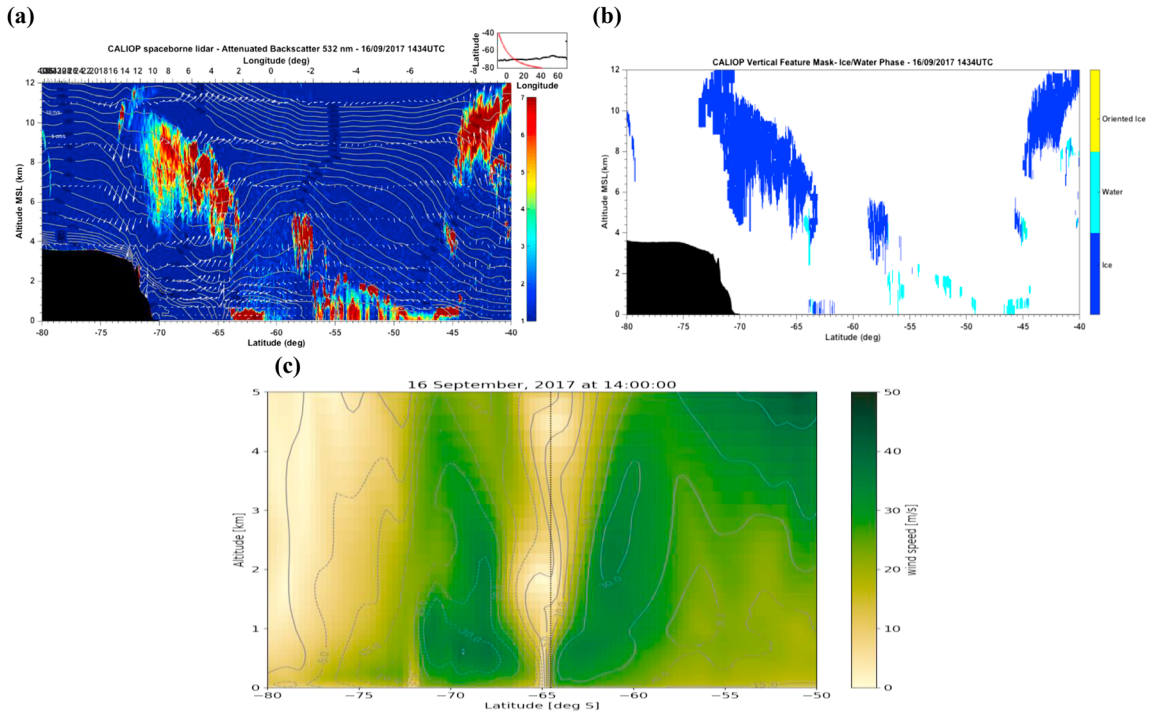

Figure 7. Cloud-Aerosol Lidar and Infrared Pathfinder Satellite Observation observations on 16 September 2017 along the yellow line in Figure 6c of backscatter coefficient (a) and ice/water phase (b). (c) Vertical cross section at 5°E of ERA5 vertical wind speed in colors. The dotted black line shows the latitude of the polynya. The gray contours represent the horizontal wind speed along the cross section every 5 m/s. The dotted contours show the southeasterly winds, and the filled contours show the northwesterlies. CALIOCloud-Aerosol Lidar with Orthogonal Polarization.

5. Characteristics of the Atmosphere Above the Polynya

The CALIPSO satellite passed over the polynya area on 16 September 2017 at 1400 UTC crossing directly over the convergence zone and the freshly opened polynya (yellow line in Figure 6c). Observations of the composition of the atmosphere above the polynya area by backscatter reflectivity revealed the presence of two layers associated with high reflectivity (Figure 7a) and composed mainly of ice (Figure 7b). The first layer is located between the surface and 700 m in altitude and stretches over 60–65°S, just above the polynya (Figure 6c and 7a). It is composed of ice crystals associated with moderated aerosol optical depth (AOD) values below 1 (Figure 8a). The fragments of ice in this layer are bigger in size than the two wavelengths 532 and 1,064 nm since their AOD does not vary with wavelength (Figures 8b and 8c). From the depolarization ratio (15% to 25%, Figure 8d), we conclude that the ice fragments in this layer are not uniform in shape, moderate depolarization ratio being associated with irregularly shaped ice crystals (e.g., Hu, 2007). The ice fragments in this layer are thought to be fragments of snow that have been uplifted into the atmosphere by strong turbulent winds associated with the violent storm described in the previous section. This process needs to be investigated further by means of modeling and observations.

The second layer of enhanced reflectivity is located between 4 and 12 km in altitude and stretches over 64–70°S (Figure 7a). It was found that this layer is also composed of ice (Figure 7b) and associated with much larger AOD values (4 to 5, Figure 8f) than the layer near the surface implying a much denser and optically thicker ice crystal cloud (Figures 8f and 8g). In this layer, the ice crystals are nonspherical but uniform in shape being associated with a depolarization ratio higher than 25% (Figure 8 h), which is in agreement with the shape in form of short sticks of ice crystals found in tropospheric clouds (e.g., Bromwich et al., 2012). This layer most probably resulted from the formation of ice crystals due of the strong updrafts over the polynya area. A vertical cross-section of ERA5 wind speeds along 5°E shows that two cores of strong opposing-winds of about 30 m/s were present on each side of the trough at 65°S (Figure 7c). Strong vertical updraft resulting from the horizontal convergence of two opposing flows is evident in the vertical cross section of winds along 5°E where weak horizontal winds reaching 0 m/s can be seen at the location of the convergence line along

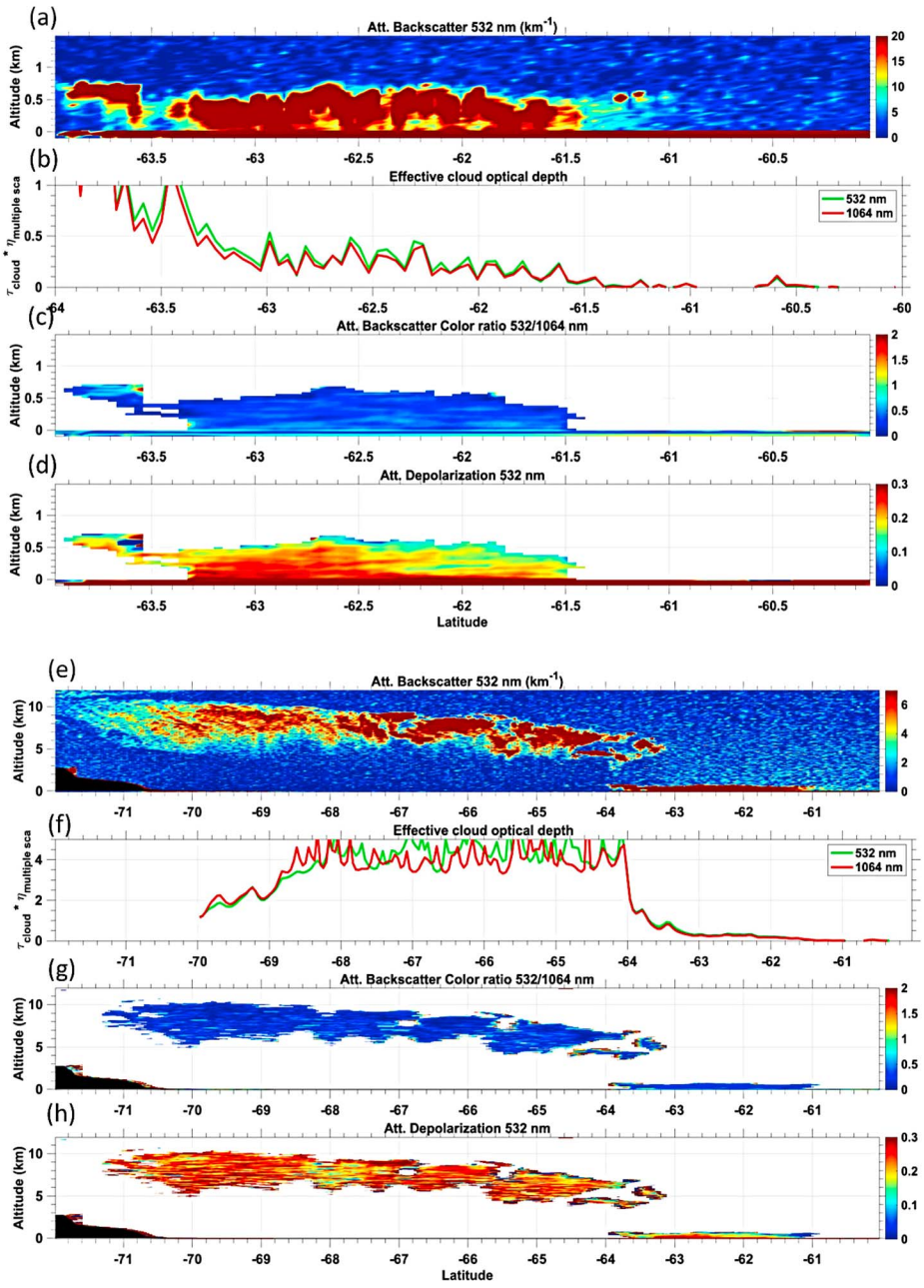

Figure 8. Properties of clouds derived from Cloud-Aerosol Lidar and Infrared Pathfinder Satellite Observation lidar measurements on 16 September 2017 at 1434 UTC at 60–64°S: (a) Transect of vertical profiles of attenuated backscatter at 532 nm, (b) effective cloud optical depth (multiplied by a multiple scattering coefficient which typically varies between 0.2 and 0.5 for clouds) derived from the attenuation of the sea surface lidar echo below clouds with respect to cloud free conditions (measured at 60.5°S), (c) attenuated backscatter color ratio between measurements at 532 and 1,064 nm, and (d) depolarization ratio at 532 nm. (e–h) The same as (a)–(d), respectively, but for the upper cloud layer located between 64° and 72°S.

the trough and over the polynya (Figure 7c), inferring the extreme dynamical forcing endured by the sea ice at the convergence zone of these two opposing surface winds.

Based on these observations, the two clouds of ice crystals observed over the polynya area do not seem to have the same origin. The cloud near the surface is most probably the result of snow uplift from the surface by turbulent winds, whereas the upper-level cloud was formed as a result of strong updrafts at the

convergence zone. The processes underlying the cloud formation at and during the opening of the polynya remain unclear, and more observations are needed for a better characterization.

6. Conclusions

In this study, we show that the opening of the Maud Rise polynya was triggered by anomalous atmospheric circulation over the Weddell and Lazarev Seas associated with an anomalously high atmospheric pressure over the Southwest Atlantic and an anomalously low pressure over the Weddell Sea and Bellingshausen Seas. These conditions occurred under a positive SAM index and a pronounced ZW3 pattern where the ZW3 index for winter 2017 was the most positive one on record. The atmospheric anomalies around the Weddell Sea were part of an Antarctic-wide amplification of the mean wave number 3 pattern, resulting in more intrusions of midlatitude warm air into the continent. This resulted in a strong meridional transport of warm and moist air masses toward the Weddell Sea associated with strong and frequent cyclones along the coast due to orographic blocking. The consecutive cyclones and their associated fronts, turbulent and cyclonic surface winds, exerted dynamical forcing on the sea ice in the Lazarev Sea as they propagated eastward. Our analysis shows that the opening of the polynya first occurred on 13 September when a strong cyclone spanned the Lazarev Sea, remained stationary for 12 hr as a result of the blocking ridge to the northeast, and was associated with cyclonic winds at the surface exceeding 25 m/s at either side of the cyclone center. The cyclone-induced winds caused divergence in the ice motion, leading to an ice-free area over the Maud Rise. The size of the polynya increased 3 days after its opening as a result of the passage of a deep trough that also developed into a strong cyclone. The polynya was located underneath a convergence zone (characterized by almost nonexistent winds, less than 2 m/s) between two opposing strong winds exceeding 22 m/s at either side of the trough. The strong convergence led to the formation of ice crystal clouds in the atmosphere between 4 and 12 km. The layer of ice above the polynya along the convergence zone was seen in CALIPSO satellite observations. The strongest surface winds are seen near the edges of the polynya where they impose strong stress on the sea ice in divergent directions leading to a rapid growth of the ice-free area in the middle of the ice pack. The dynamical removal of the sea ice from this region just before the ice melt, when the ocean surface density stratification is weak, may have triggered strong positive feedbacks (Gordon, 1991) that led to a larger polynya during the spring months.

Despite the fact that the ocean circulation around the Maud Rise acts as a permanent preconditioning for the occurrence of the Maud Rise polynya, the polynya does not occur often. Our results show that for the opening to occur, polar cyclones and their associated strong cyclonic winds near the surface can be the trigger through ice divergence caused by cyclonic winds.

This study demonstrates that strong winds can open midsea polynyas in the same way they open coastal polynyas, providing they are cyclonic or opposed in direction along a convergence zone in order to create divergence in the ice field in the middle of the ice pack, the ice being dragged 30° in average to the left of the wind flow. For comparison, the katabatic winds that open coastal polynyas are associated with wind speeds of 10 m/s on average. Cyclonic winds over the Lazarev Sea exceeded 24 m/s. The occurrence of such strong cyclones over the ice pack, south of the ice edge, occurred under a ZW3-like atmospheric circulation. The meridional transport of heat to the Weddell Sea pushed the atmospheric meridional temperature gradient poleward and resulted in a temperature gradient and associated instability over the ice pack to the south of the ice edge, whereas usually it is located near to it. Under such situations, the severe atmospheric conditions, particularly storms, which usually occur near the ice edge and impact the ice drift and dynamics, occur now over the ice pack. The resulting configuration of alternating cold and warm air masses enhanced the zonal temperature gradient and generated baroclinic instability at the frontal areas between cold and warm air flows favoring the maintenance of intense cyclones over time and distance.

In a similar way to the formation of coastal polynyas, which are a result of strong katabatic winds that push the ice away from the coast, we demonstrated here that open-ocean polynyas can also be atmospheric driven and their initial opening results from strong cyclonic winds that create divergence in the ice field. Our results showed that atmospheric forcing on sea ice, induced by cyclonic winds were critical to trigger the opening of the polynya, but it is most probable that ocean convection and dynamics have played important role in maintaining the polynya open throughout the winter months and influence its lifetime and size variation.

These results are in agreement with those found for the occurrence of the Cosmonaut polynya in the Cosmonaut Sea in Antarctica. Bailey et al. (2004) examined the conditions for the occurrence of the mid-ocean polynya in the Cosmonaut Sea by means of modeling. In their experiments, a polynya was simulated in the open ocean, away from the coast. They found that the formation of this polynya cannot be achieved by oceanic forcing alone. The simulation only produced a polynya when the sea ice was advected out of the region by atmospheric forcing. This is in line with the findings by Arbetter et al. (2004) who established a climatology of the occurrence of the Cosmonaut polynya and its link to atmospheric conditions by mean of reanalysis and satellite observations. They found that, along with the drop in sea ice area, there is a drop in sea level pressure as well as an increase in atmospheric wind divergence when the Cosmonaut Sea polynya is present and that in some months, the sea ice area decrease is preceded by the passage of an atmospheric low pressure system 1–2 days earlier.

The ice-free area tends to occur at the frontal region between two opposing flows in the vicinity of their convergence zone. Such particular conditions are favored by frequent and intense cyclones crossing over the ice pack and by strong temperature gradients and frontogenesis. Both situations are fostered by an enhanced meridional heat transport. Our results show that the atmospheric conditions in 2017, associated with an amplified atmospheric ZW3 and characterized by strong meridional transport of heat, impacted the sea ice conditions in several ways: (1) the enhancement of strong zonal temperature gradients between the different sectors, leading to baroclinic instability that generates dynamically strong storms, which in turn impacts the sea ice dynamics; (2) the occurrence of intense and frequent storms that are able to reach further south and penetrate deeper over the ice pack; and (3) the shift of the horizontal temperature gradient (and the cyclones that form across it) south of the ice edge in the Weddell Sea, enabling cyclones to form over the ice pack and force the sea ice conditions.

The intensification of the activity of polar cyclones is linked to the poleward shift of the extratropical storm track, and this link is pronounced under future warming climate conditions (e.g., Fyfe, 2003). Furthermore, a poleward shift of the cyclone activity results in a reduced sea ice extent (e.g., Pezza et al., 2008; Simmonds & Wu, 1993), a situation similar to the one observed in 2016 and 2017 (e.g., Schlosser et al., 2018). When the sea ice extent is reduced, preferable polynya areas located in the ice pack (i.e., the Maud Rise) become closer to the ice edge and hence to the cyclogenesis zone. Given the link between polynya occurrence and cyclones we demonstrate in this study, it remains to be seen how polynya frequency evolves in the future given the changes predicted in the SAM, in the storm track, and in the sea ice extent. Finally, the link between the frequency of polynyas and the ZW3 pattern is to be addressed in future work.

Acknowledgments
The European Centre for Medium-Range Weather Forecasts (ECMWF) is acknowledged for making the meteorological analyses available from their data server (https://apps.ecmwf.int/datasets/). The National Snow and Ice Data Center (NSIDC) is acknowledged for making the satellite observations on sea ice available from their data server (https://nsidc.org/data/icesat/data.html). The CALIPSO data used in this study are available at the website (https://www-calipso.larc.nasa.gov/tools/data_avail/). We acknowledge the use of imagery provided by services from the Global Imagery Browse Services (GIBS), operated by NASA's Earth Science Data and Information System (ESDIS) Project. The authors wish to thank two anonymous reviewers for their valuable comments and suggestions. This research work was supported by the NYU Abu Dhabi Research Institute in the UAE, grant 1204.

References

Arbetter, T. E., Lynch, A. H., & Bailey, D. A. (2004). Relationship between synoptic forcing and polynya formation in the Cosmonaut Sea: 1. Polynya climatology. *Journal of Geophysical Research*, *109*, C04022. https://doi.org/10.1029/2003JC001837

Bailey, D. A., Lynch, A. H., & Arbetter, T. E. (2004). Relationship between synoptic forcing and polynya formation in the Cosmonaut Sea: II. Regional climate model simulations. *Journal of Geophysical Research*, *109*, C04023. https://doi.org/10.1029/2003JC001838

Bernardello, R., Marinov, I., Palter, J. B., Galbraith, E. D., & Sarmiento, J. L. (2014). Impact of Weddell Sea deep convection on natural and anthropogenic carbon in a climate model. *Geophysical Research Letters*, *41*, 7262–7269. https://doi.org/10.1002/2014GL061313

Bou Karam, D., Flamant, C., Cuesta, J., Pelon, J., & Williams, E. (2010). Dust emission and transport associated with a Saharan depression: The February 2007 case. *Journal of Geophysical Research*, *115*, D00H27. https://doi.org/10.1029/2009JD012390

Bromwich, D. H., Nicolas, J. P., Hines, K. M., Kay, J. E., Key, E. L., Lazzara, M. A., et al. (2012). Tropospheric clouds in Antarctica. *Reviews of Geophysics*, *50*, RG1004. https://doi.org/10.1029/2011RG000363

Bromwich, D. H., Steinhoff, D. F., Simmonds, I., Keay, K., & Fogt, R. L. (2011). Climatological aspects of cyclogenesis near Adélie Land, Antarctica. *Tellus Series A: Dynamic Meteorology and Oceanography*, *63*(5), 921–938.

Carsey, F. D. (1980). Microwave observation of the Weddell Polynya. *Monthly Weather Review*, *108*(12), 2032–2044. https://doi.org/10.1175/1520-0493(1980)108,2032:MOOTWP.2.0.CO;2

Cavalieri, D. J., & Parkinson, C. L. (2008). Antarctic sea ice variability and trends, 1979–2006. *Journal of Geophysical Research*, *113*, C07004. https://doi.org/10.1029/2007JC004564

Clem, K. R., Barreira, S., & Fogt, R. L. (2017). Atmospheric circulation. In J. Blunden & D. S. Arndt (Eds.), *State of the Climate 2016*, *Bulletin of the American Meteorological Society* (Vol. 98, pp. 156–158). https://doi.org/10.1175/2017BAMSStateoftheClimate.1

Comiso, J. C. (1986). Characteristics of Arctic winter sea ice from satellite multispectral microwave observations. *Journal of Geophysical Research*, *91*(C1), 975–994. https://doi.org/10.1029/JC091iC01p00975

Comiso, J. C., Cavalieri, D. J., Parkinson, C. L., & Gloersen, P. (1997). Passive microwave algorithms for sea ice concentration: A comparison of two techniques. *Remote Sensing of Environment*, *60*(3), 357–384. https://doi.org/10.1016/S0034-4257(96)00220-9

Cuesta, J., Marsham, J. H., Parker, D. J., & Flamant, C. (2009). Dynamical mechanisms controlling the vertical redistribution of dust and the thermodynamic structure of the west Saharan atmospheric boundary layer during summer. *Atmospheric Science Letters*, *10*(1), 34–42. https://doi.org/10.1002/asl.207

Davies, H. C. (1997). Emergence of the mainstream cyclogenesis theories. *Meteorologische Zeitschrift*, *6*, 261–274.

Dee, D. P., Uppala, S. M., Simmons, A. J., Berrisford, P., Poli, P., Kobayashi, S., et al. (2011). The ERA-Interim reanalysis: Configuration and performance of the data assimilation system. *Quarterly Journal of the Royal Meteorological Society*, *137*(656), 553–597. https://doi.org/10.1002/qj.828

Dufour, C. O. A., Morrison, K., Griffies, S. M., Frenger, I., Zanowski, H., & Winton, M. (2017). Preconditioning of the Weddell Sea polynya by the ocean mesoscale and dense water overflows. *Journal of Climate*, *30*(19), 7719–7737. https://doi.org/10.1175/JCLI-D-16-0586.1

Eady, E. T. (1949). Long waves and cyclone waves. *Tellus*, *1*(3), 33–52.

Francis, D., Eayrs, C., Chaboureau, J.-P., Mote, T., & Holland, D. (2018). Polar jet associated circulation triggered a Saharan cyclone and derived the poleward transport of the African dust generated by the cyclone. *Journal of Geophysical Research: Atmospheres*, *123*, 11,899–11,917. https://doi.org/10.1029/2018JD029095

Fyfe, J. C. (2003). Extratropic Southern Hemisphere cyclones: Harbingers of climate change? *Journal of Climate*, *16*(17), 2802–2805. https://doi.org/10.1175/1520-0442(2003)016<2802:ESHCHO>2.0.CO;2

Gordon, A. L. (1991). Two stable modes of Southern Ocean winter stratification. In J. Gascard & P. Chu (Eds.), *Deep Convection and Water Mass Formation in the Ocean* (pp. 17–35). Elsevier.

Gordon, A. L. (1998). Western Weddell Sea thermohaline stratification. In S. Jacobs, & R. Weiss (Eds.), *Ocean, Ice, and Atmosphere: Interactions at the Antarctic Continental Margin* (pp. 215–240). Washington, DC: American Geophysical Union.

Hersbach H., & Dee D. (2016). ERA-5 reanalysis is in production. ECMWF newsletter, number 147, Spring 2016, p.7.

Holland, D. M. (2001). Explaining the Weddell polynya—A large ocean eddy shed at Maud Rise. *Science*, *292*(5522), 1697–1700. https://doi.org/10.1126/science.1059322

Holland, P. R., & Kwok, R. (2012). Wind-driven trends in Antarctic sea-ice drift. *Nature Geoscience*, *5*, 872–875. https://doi.org/10.1038/ngeo1627

Hu, Y. (2007). Depolarization ratio-effective lidar ratio relation: Theoretical basis for space lidar cloud phase discrimination. *Geophysical Research Letters*, *34*, L11812. https://doi.org/10.1029/2007GL029584

Hurrell, J. H., van Loon, H., & Shea, D. (1998). The mean state of the troposphere. *Southern Hemisphere Meteorological Monograph #49* (pp. 1–46). American Met. Soc.

Irving, D., & Simmonds, I. (2015). A novel approach to diagnosing Southern Hemisphere planetary wave activity and its influence on regional climate variability, Journal of Climate. *American Meteorological Society*, *28*(23), 9041–9057. https://doi.org/10.1175/JCLI-D-15-0287.1

Kolstad, E. W. (2011). A global climatology of favourable conditions for polar lows. *Quarterly Journal of the Royal Meteorological Society*, *137*(660), 1749–1761. https://doi.org/10.1002/qj.888

Kottmeier, C., Olf, J., Frieden, W., & Roth, R. (1992). Wind forcing and ice motion in the Weddell Sea region. *Journal of Geophysical Research*, *97*, 20,373–20,383. https://doi.org/10.1029/92JD02171

Kottmeier, C., & Sellmann, L. (1996). Atmospheric and oceanic forcing of Weddell Sea ice motion. *Journal of Geophysical Research*, *101*, 20,809–20,824. https://doi.org/10.1029/96JC01293

Kurtakoti, P., Veneziani, M., Stössel, A., & Weijer, W. (2018). Preconditioning and formation of Maud Rise polynyas in a high-resolution Earth system model. *Journal of Climate*, *31*(23), 9659–9678. https://doi.org/10.1175/JCLI-D-18-0392.1

Kwok, R., Pang, S. S., & Kacimi, S. (2017). Sea ice drift in the Southern Ocean: Regional patterns, variability and trends. *Elementa: Science of the Anthropocene*, *5*, 1–16. https://doi.org/10.1525/elementa.226

Kwok, R., Spreen, G., & Pang, S. (2013). Arctic sea ice circulation and drift speed: Decadal trends and ocean currents. *Journal of Geophysical Research: Atmospheres*, *118*, 2408–2425. https://doi.org/10.1002/jgrc.20191

Lavergne, T., Eastwood, S., Teffah, Z., Schyberg, H., & Breivik, L.-A. (2010). Sea ice motion from low resolution satellite sensors: An alternative method and its validation in the Arctic. *Journal of Geophysical Research*, *115*, C10032. https://doi.org/10.1029/2009JC005958

Leppäranta, M. (2011). *The Drift of Sea Ice*. Berlin Heidelberg: Springer. https://doi.org/10.1007/978-3-642-04683-4

Lindzen, R. S., & Farrell, B. (1980). A simple approximate result for the maximum growth rate of baroclinic instabilities. *Journal of the Atmospheric Sciences*, *37*(7), 1648–1654. https://doi.org/10.1175/1520-0469(1980)037<1648:ASARFT>2.0.CO;2

Lubin, D., Wittenmyer, R. A., Bromwich, D. H., & Marshall, G. J. (2008). Antarctic Peninsula mesoscale cyclone variability and climatic impacts influenced by the SAM. *Geophysical Research Letters*, *35*, L02808. https://doi.org/10.1029/2007GL032170

Marshall, G. (2003). Trends in the Southern Annular Mode from observations and reanalyses. *Journal of Climate*, *16*(24), 4134–4143. https://doi.org.10.1175/1520-0442(2003)016h4134:TITSAMi2.0.CO;2

Martin, T., Park, W., & Latif, M. (2013). Multi-centennial variability controlled by Southern Ocean convection in the Kiel Climate Model. *Climate Dynamics*, *40*(7-8), 2005–2022. https://doi.org/10.1007/s00382-012-1586-7

Martin, T., Park, W., & Latif, M. (2015). Southern Ocean forcing of the North Atlantic at multi-centennial time scales in the Kiel Climate Model. *Deep-Sea Research Part II: Topical Studies in Oceanography*, *114*, 39–48. https://doi.org/10.1016/j.dsr2.2014.01.018

Matear, R., O'Kane, T., Risbey, J., & Chamberlain, M. (2015). Sources of heterogeneous variability and trends in Antarctic sea-ice. *Nature Communications*, *6*. https://doi.org.10.1038/ncomms9656

Mazloff, M. R., Sallée, J.-B., Menezes, V. V., Macdonald, A. M., Meredith, M. P., Newman, L., et al. (2017). Southern Ocean, in: *State of the Climate 2016*, edited by: Blunden, J. and Arndt, D. S., Bulletin of the American Meteorological Society, *98*, 166–167, https://doi.org/10.1175/2017BAMSStateoftheClimate.1

Meier, W., Fetterer, F., Savoie, M., Mallory, S., Duerr, R., & Stroeve, J. (2017). NOAA/NSIDC Climate Data Record of passive microwave sea ice concentration, version 3. [Antarctic, daily, monthly]. Boulder, Colorado USA. NSIDC: National Snow and Ice Data Center. doi: https://doi.org/10.7265/N59P2ZTG. [Date Accessed: 22 April, 2018].

Meier, W., Fetterer, F., & Windnagel, A. K. (2017). Near-real-time NOAA/NSIDC climate data record of passive microwave sea ice concentration, version 1. [Antarctic, daily, monthly]. doi: https://doi.org/10.7265/N5FF3QJ6. [Date Accessed: 22 April, 2018].

Moore, G. W. K., Alverson, K., & Renfrew, I. A. (2002). A reconstruction of the air–sea interaction associated with the Weddell Polynya. *Journal of Physical Oceanography*, *32*(6), 1685–1698. https://doi.org/10.1175/1520-0485(2002)032,1685:AROTAS.2.0.CO;2

Morales Maqueda, M. A., Willmott, A. J., & Biggs, N. R. T. (2004). Polynya dynamics: A review of observations and modeling. *Reviews of Geophysics*, *42*, RG1004. https://doi.org/10.1029/2002RG000116

Nansen, F. (1902). The Oceanography of the North Polar Basin. *Norwegian North Polar Expedition 1893±1896*, *Scienti®c Results* (Vol. III, pp. 9). Kristiania, Norway: Longman Green & Co.

Nihashi, S., & Ohshima, K. I. (2015). Circumpolar mapping of Antarctic coastal polynyas and landfast sea ice: Relationship and variability. *Journal of Climate*, *28*(9), 3650–3670. https://doi.org/10.1175/JCLI-D-14-00369.1

Orlanski, I. (1975). A rational subdivision of scales for atmospheric processes. *Bulletin of the American Meteorological Society*, *56*(5), 527–530.

Parkinson, C. L. (2004). Southern Ocean sea ice and its wider linkages: Insights revealed from models and observations. *Antarctic Science*, *16*(4), 387–400. https://doi.org/10.1017/S0954102004002214

Pezza, A. B., Durrant, T., Simmonds, I., & Smith, I. (2008). Southern Hemisphere synoptic behavior in extreme phases of SAM, ENSO, sea ice extent, and southern Australia rainfall. *Journal of Climate*, *21*(21), 5566–5584. https://doi.org/10.1175/2008JCLI2128.1

Pope, J. O., Holland, P. R., Orr, A., Marshall, G. J., & Phillips, T. (2017). The impacts of El Niño on the observed sea ice budget of West Antarctica. *Geophysical Research Letters*, *44*, 6200–6208. https://doi.org/10.1002/2017GL073414

Raphael, M. N. (2004). A zonal wave 3 index for the Southern Hemisphere. *Geophysical Research Letters*, *31*, L23212. https://doi.org/10.1029/2004GL020365

Raphael, M. N. (2007). The influence of atmospheric zonal wave three on Antarctic sea ice variability. *Journal of Geophysical Research*, *112*, D12112. https://doi.org/10.1029/2006JD007852

Raphael, M. N., & Hobbs, W. (2014). The influence of the large-scale atmospheric circulation on Antarctic sea ice during ice advance and retreat seasons. *Geophysical Research Letters*, *41*, 5037–5045. https://doi.org/10.1002/2014GL060365

Rasmussen, E. A., & Turner, J. (2003). *Polar Lows: Mesoscale Weather Systems in the Polar Regions*, (p. 612). Cambridge, UK: Cambridge University Press. https://doi.org/10.1017/CBO9780511524974

Reed, R. J. (1979). Cyclogenesis in polar air streams. *Monthly Weather Review*, *107*(1), 38–52. https://doi.org/10.1175/1520-0493(1979)107<0038:CIPAS>2.0.CO;2

Reed, R. J., & Duncan, C. N. (1987). Baroclinic instability as a mechanism for the serial development of polar lows. *Tellus*, *39*(4), 376–384. https://doi.org/10.3402/tellusa.v39i4.11766

Reid, P., Stammerjohn, S., Massom, R. A., Lieser, J. L., Barreira, S., & Scambos, T. (2017). Sea ice extent, concentration, and seasonality, in: *State of the Climate 2016*, edited by: et al., Bulletin of the American Meteorological Society, *98*, 163–166, https://doi.org/10.1175/2017BAMSStateoftheClimate.1

Rudeva, I., & Gulev, S. K. (2007). Climatology of cyclone size characteristics and their changes during the cyclone life cycle. *Monthly Weather Review*, *135*(7), 2568–2587. https://doi.org/10.1175/MWR3420.1

Schemm, S. (2018). Regional trends in weather systems help explain Antarctic sea ice trends. *Geophysical Research Letters*, *45*, 7165–7175. https://doi.org/10.1029/2018GL079109

Schemm, S., & Sprenger, M. (2015). Frontal-wave cyclogenesis in the North Atlantic—A climatological characterisation. *Quarterly Journal of the Royal Meteorological Society*, *141*(693), 2989–3005. https://doi.org/10.1002/qj.2584

Schlosser, E., Haumann, F. A., & Raphael, M. N. (2018). Atmospheric influences on the anomalous 2016 Antarctic sea ice decay (2018). *The Cryosphere*, *12*(3), 1103–1119. https://doi.org/10.5194/tc-12-1103-2018

Schlosser, E., Powers, J. G., Duda, M. G., & Manning, K. W. (2011). Interaction between Antarctic sea ice and synoptic activity in the circumpolar trough: Implications for ice-core interpretation. *Annals of Glaciology*, *52*(57), 9–17.

Shimada, U., Wada, A., Yamazaki, K., & Kitabatake, N. (2014). Roles of an upper-level cold vortex and low-level baroclinicity in the development of polar lows over the Sea of Japan. *Tellus A: Dynamic Meteorology and Oceanography*, *66*(1). https://doi.org/10.3402/tellusa.v66.24694

Simmonds, I., Burke, C., & Keay, K. (2008). Arctic climate change as manifest in cyclone behavior. *Journal of Climate*, *21*(22), 5777–5796. https://doi.org/10.1175/2008JCLI2366.1

Simmonds, I., & Wu, X. R. (1993). Cyclone behavior response to changes in winter Southern Hemisphere sea-ice concentration. *Quarterly Journal of the Royal Meteorological Society*, *119*(513), 1121–1148. https://doi.org/10.1002/qj.49711951313

Stoll, P. J., Graversen, R. G., Noer, G., & Hodges, K. (2018). An objective global climatology of polar lows based on reanalysis data. *Quarterly Journal of the Royal Meteorological Society*, *144*(716), 2099–2117. https://doi.org/10.1002/qj.3309

Swart, S., Cambell, E. C., Heuze, C. H., Johnson, K., Lieser, J. L., Masson, R., et al. (2018). Litmus or sea ice anomaly? Sidebar, State of the Climate. *Bulletin of the American Meteorological Society*, *99*(8), 1527–1539. https://doi.org/10.1175/BAMS-D-18-0173.1

Turner, J., Harangozo, S. A., Marshall, G. J., King, J. C., & Colwell, S. R. (2002). Anomalous atmospheric circulation over the Weddell Sea, Antarctica during the austral summer of 2001/02 resulting in extreme sea ice conditions. *Geophysical Research Letters*, *29*(24), 2160. https://doi.org/10.1029/2002GL015565

Uccellini, L. W. (1990). Processes contributing to the rapid development of extratropical cyclones. In C. W. Newton, & E. O. Holopainen (Eds.), *Extratropical Cyclones* (pp. 81–105). Boston, MA: American Meteorological Society. https://doi.org/10.1007/978-1-944970-33-8_6

van Loon, H., & Jenne, R. L. (1972). The zonal harmonic standing waves in the Southern Hemisphere. *Journal of Geophysical Research*, *77*(6), 992–1003. https://doi.org/10.1029/JC077i006p00992

Wagner, J. S., Gohm, A., Dörnbrack, A., & Schäfler, A. (2011). The mesoscale structure of a polar low: Airborne lidar measurements and simulations. *Quarterly Journal of the Royal Meteorological Society*, *137*(659), 1516–1531. https://doi.org/10.1002/qj.857

Wang Z, Turner J, Sun B, Li B, Liu C., (2014), Cyclone-induced rapid creation of extreme Antarctic sea ice conditions. Scientific Reports. 2014;4:5317. doi:https://doi.org/10.1038/srep05317.

Watanabe, S. I., & Niino, H. (2014). Genesis and development mechanisms of a polar mesocyclone over the Japan Sea. *Monthly Weather Review*, *142*(6), 2248–2270. https://doi.org/10.1175/MWR-D-13-00226.1

Weijer, W., Veneziani, M., Stossel, A., Hecht, M. W., Jeffery, N., Jonko, A., et al. (2017). Local atmospheric response to an open-ocean polynya in a high-resolution climate model. *Journal of Climate*, *30*(5), 1629–1641. https://doi.org/10.1175/JCLI-D-16-0120.1

Winker, D. M., Pelon, J., & McCormick, M. P. (2003). The CALIPSO mission: Spaceborne lidar for observation of aerosols and clouds. *Proceedings of SPIE*, *4893*, 1–11.

Yanase, W., & Niino, H. (2007). Dependence of polar low development on baroclinicity and physical processes: An idealized high-resolution numerical experiment. *Journal of the Atmospheric Sciences*, *64*(9), 3044–3067. https://doi.org/10.1175/JAS4001.1

Zanowski, H., Hallberg, R., & Sarmiento, J. L. (2015). Abyssal ocean warming and salinification after Weddell polynyas in the GFDL CM2g coupled climate model. *Journal of Physical Oceanography*, *45*(11), 2755–2772. https://doi.org/10.1175/JPO-D-15-0109.1